KSÜ Mühendislik Bilimleri Dergisi, 27(1), 2024
Araştırma Makalesi

KSU J Eng Sci, 27(1), 2024
Research Article

Kahramanmaras Sutcu Imam University
Journal of Engineering Sciences

Geliş Tarihi : 04.09.2023
Kabul Tarihi : 31.10.2023

Received Date : 04.09.2023
Accepted Date :31.10.2023

A NUMERICAL ANALYSIS ON THE SUBMICRON- AND MICRON-SIZED PARTICLE SEDIMENTATION IN A WIRE-TO-PLATE ELECTROSTATIC PRECIPITATOR

TELDEN-PLAKAYA TÜRDE BİR ELEKTROSTATİK ÇÖKTÜRÜCÜDE MİKRONALTI- VE MİKRON-BOYUTLU PARTİKÜL BİRİKİMİNİN NÜMERİK ANALİZİ

Orçun EKİN[1*] (ORCID: 0000-0002-6779-885X)

[1] Aydın Adnan Menderes Üniversitesi, Makine Mühendisliği Bölümü, Aydın, Türkiye

* Corresponding Author/Sorumlu Yazar: Orçun EKİN, orcun.ekin@adu.edu.tr

ABSTRACT

Electrostatic precipitators (ESPs) are frequently utilized in collecting fine organic and inorganic materials from continuous liquid with few moving parts and high efficiency using electrically charging the particles. In this study, cross-sectional 2D geometry of a wire-to-plate electrostatic precipitator the parametric data of which originally published elsewhere was numerically modeled and validated to investigate submicron-micron particle charging in terms of diffusion and field charging mechanisms and precipitation behavior of particles with detailed electric field properties. Electric field, gas flow, and particle trajectory equations are coupled and solved in a multiphysics solver. Particle tracking is realized with the Lagrangian approach. Results indicate variations in electric field strength and space charge density between corona electrodes, with space charge present in the entire precipitation channel. Between two different charging mechanisms, diffusion charging prevails for charge accumulated on submicron particles, whereas field charging becomes dominant for particles larger than 1μm diameter. However, for the ESP configuration considered in this study, particles reach a charge saturation in less than 0.7 seconds, regardless of their size. Although calculated precipitation efficiencies for micron-sized particles can reach to 100%, efficiencies for submicron particle range drop with increasing particle size, as diffusion charging rapidly loses its effectiveness, in 50-250nm range.

Keywords: Computational Fluid Dynamics, Corona Discharge, Discrete Element Modeling, Electrostatic Precipitation, Particle Trajectories.

ÖZET

Elektrostatik çöktürücüler (ESP), küçük boyutlu organik ve inorganik maddelerin sürekli akışkan içerisinden elektriksel olarak yüklenmeleri suretiyle yüksek hassasiyetle ayrıştırılmalarında yararlanılan, yapılarında asgari hareketli aksam bulunduran cihazlardır. Bu çalışmada, deneysel verileri daha önce bir başka kaynakta yayınlanmış olan telden-plakaya tipteki elektrostatik çöktürücü sonlu elemanlar yöntemi ile 2 boyutlu kesit geometri olarak modellenmiş ve mikron- ve mikron-altı partiküllerin alansal ve difüzyon mekanizmaları ile elektriksel olarak yüklenmelerinin, ayrıca partikül çökelme davranışlarının detaylı elektrik alan özellikleri kapsamında incelenmesi amacıyla valide edilmiştir. Elektrik alan, gaz akışı ve partikül yörünge denklemleri bağlaşık hale getirilerek multifizik ortamında çözdürülmüştür. Partikül takibi Lagrange yaklaşımı ile modellenmiştir. Modelin sonuçları korona elektrotları arasında gerek elektrik alan kuvvetinde gerekse uzay yük yoğunluğunda kayda değer farklılıklar olduğunu ve uzay yükünün tüm çökelme kanalına yayıldığını ortaya koymaktadır. İki yüklenme mekanizmasından, difüzyon mekanizmasının mikron-altı partiküllerde oluşan yük birikiminde etkili iken alansal yüklenmenin daha ziyade 1μm'den daha büyük partiküllerde ön planda olmaktadır. Bununla birlikte, çalışma kapsamında dikkate alınmış olan ESP konfigürasyonunda partiküller 0.7 saniyeden kısa süre içerisinde elektriksel yük bakımından doygun hale gelmektedirler. Mikron boyutlu partiküllerin çökelme verimleri çapa bağlı olarak %100 mertebesine ulaşmakla

ToCite: EKİN, O., (2024). A NUMERICAL ANALYSIS ON THE SUBMICRON- AND MICRON-SIZED PARTICLE SEDIMENTATION IN A WIRE-TO-PLATE ELECTROSTATIC PRECIPITATOR. *Kahramanmaraş Sütçü İmam Üniversitesi Mühendislik Bilimleri Dergisi*, 27(1),78-91.

birlikte mikron-altı partiküllerde artan partikül çapı ile difüzyon yüklenme mekanizması etkisini hızla kaybetmekte, dolayısıyla 50-250nm arasındaki partiküllerin çökelme verimlerinde önemli düşüş gözlenmektedir.

Anahtar Kelimeler: Ayrık Eleman Modelleme, Elektrostatik Çökeltme, Hesaplamalı Akışkanlar Dinamiği, Korona Deşarjı, Partikül Yörüngeleri.

INTRODUCTION

Electrostatic precipitation (ESP) is a technique, where the electrostatic body forces accumulated on the submicron and micron particles are used for particle sedimentation. EPSs are commonly used in areas and processes in which purifying air, or other gases, is required [1]. One characteristic of the EPS is that very high collection efficiencies are achieved (usually >99%) for micron-sized particles [2], with relatively low-pressure losses through the precipitation channel, typically lower than 1000 Pa. These properties, along with a typically low number of moving parts employed, make these devices a robust and cost-efficient method in particle-laden fluid treatment applications [3]. Precipitation of submicron and micron-sized particles on surfaces by way of electrical manipulation offers is promising for in-line particle sedimentation processes in the industry and many household applications. On the other hand, controlling the parameters that govern high-intensity corona discharges, resulting charge accumulation on particles, and finally the sedimentation characteristics of particles with specific physical properties require a thorough understanding of the process, which implies its multidisciplinary character.

Corona discharge is the principal process in ESP, as the mechanism behind particle charging, hence the high precipitation efficiency is primarily related to the number of ions generated and transported into the domain as a result of corona discharge [4]. Several studies focus on the investigation of temperature effects on discharge characteristics in DC corona configurations [5], [6] and the effects of electric potential on fine aerosol particle precipitation in positive DC corona discharges for cleaning indoor air. The increasing level of temperature negatively affects the energy consumption of the system [7]-[9].

As stated previously, the understanding and design of an ESP with high precipitation efficiency require a detailed understanding of different aspects of the process, such as the electrostatic characteristics of the setup, the effect of the gas composition, and particle properties [10]. Experimental studies are probably the most accurate way to investigate the process, yet they might not be the most time- and resource-efficient way, given the complex character of a typical ESP application. However, as is the case in many modern engineering applications, these difficulties can be overcome using mathematical modelling. In numerical modelling, the collected data, which were first validated, can be used to study different aspects of the process [11].

In the current study, the coupled physics of ESP, namely corona discharge, forced convection of air, charge accumulation on solid particles, particle-laden flow characteristics, and particle tracking are characterized and solved, using the COMSOL Multiphysics commercial software. The model is first validated against a previous experimental study and then the precipitation efficiencies along with the electric field parameters occurring in the solution domain are investigated. The study takes a different perspective and outlines the effects of the two charging mechanisms influencing the particle precipitation. Detailed numerical studies are available on the wire-to-plane configuration, however with the emphasis generally on the electrical field properties and total precipitation figures [10, 12, 13].

MATERIAL AND METHOD

Fluid Flow

Solving the turbulent flow might prove a difficult task, despite the ever-increasing efficiency of the computing methods. The multiphysics nature of the problem requires highly refined discretization schemes, which require a great amount of computational power, even for 2D applications. As usual with systems of high complexity, certain simplifications become necessary in ESP modelling, such as incompressible flow assumption [14]. This is justified by low pressure drop along the precipitation channel [15, 16]. The time-averaged conservation equations for mass and momentum are utilized to express continuous flow of air with electrical body force calculated in a different module.

Conservation of mass is given by:

$$\frac{\partial}{\partial x_k}(\rho u_k) = 0 \tag{1}$$

Conservation of momentum is expressed as:

$$\frac{\partial}{\partial x_k}\left(\rho u_i u_k - (\mu + \mu_t)\frac{\partial u_i}{\partial x_k}\right) = -\frac{\partial p}{\partial x_i} + f_{D_i} + \rho_{ion} E_i \tag{2}$$

where ρ and ρ_{ion} represent air density and the concentration of ionic charges, respectively, u is the gas velocity, f_D is the drag coefficient, and E_i is the strength of electric field. With the normal process properties of ESPs in air purification applications, the calculated Reynolds numbers usually indicate a turbulent flow scheme [16]. Given its ability to represent turbulence flows in a wide variety of applications, the standard $\mathrm{k}-\varepsilon$ turbulence model is used in this study, to calculate the turbulent viscosity, μ_t, therefore, to solve the Reynolds-Averaged Navier Stokes equations for turbulence kinetic energy and turbulence dissipation rate [12, 17, 18].

Particulate Flow and Particle Charging

As customary in computational fluid dynamics-discrete element modeling (CFD-DEM) applications, the particle-laden flow can be described using two principal approaches: the Eulerian and the Lagrangian. The Eulerian approach treats both components of the flow (fluid and particles) as continua, whereas the Lagrangian approach considers only the fluid as continuum and the particles as discrete elements scattered in this continuous fluid. Forces acting on each individual particle are considered and the particle momentum and positions are calculated for every step of the solution. Both approaches have some advantages depending on the application [19, 20]. With the Lagrangian approach, detailed information for each individual particle injected into the solution domain: particle positions and trajectories, particle momentum, and particle fates (trapped on the surfaces, escaped the solution domain, or stagnated), are available. The Lagrangian approach can consider multiple particle types, shapes, and distribution of sizes. On the other hand, the Lagrangian approach brings a limitation on the particle volume fraction, as treating each particle separately demands very high computational capacity. Therefore, the Lagrangian approach is only utilized where the particle phase is 'dilute', compared to the continuous fluid. The Eulerian approach has the advantage of configuring mixtures with high particulate content more easily, hence preferred over the Lagrangian approach in certain applications [21, 22, 23]. In the scope of the present study, since the particulate phase is sufficiently dilute and a size-distribution of particles is available, the Lagrangian approach to particulate-phase configuration is preferred.

Particles injected into ESP are exposed to aerodynamic drag and electric body force, therefore their trajectories in the precipitation channel are determined mainly by these two factors. Due to the dispersed character of the Lagrangian particulate flow, the particle-particle interactions are ignored, thus the particle motion equation takes the form:

$$M_p \frac{dv_i}{dt} = q_p E_i + 3\pi\mu d_p(\tilde{u}_i - v_i)(1 + 0.15Re_p^{0.687}) \tag{3}$$

where M_p is the mass of an individual particle, v_i is the particle velocity, q_p is the particle charge, d_p ,s the particle diameter, $Re_p = \rho|u - v|d_p/\mu$ is particle Reynolds number. The instantaneous gas velocity, $\tilde{u}$ is a sum of two velocity components, namely the mean and fluctuating velocity. The fluctuating component is calculated through turbulent kinetic energy, as a result of time-averaged conservation equation approach. The two-way turbulence coupling is fully accounted for when the particles affect fluid flow and gas flow affects the particle trajectory. The particle momentum source term is given by [24]:

$$f_{D_i} = \sum_{k=1}^{N_J} \frac{6\dot{m}_p^k}{\pi\rho_p\left(d_p^k\right)^3} \frac{\rho\pi\left(d_p^k\right)^2}{8} \int_{t_{in}}^{t_{out}} C_D\left|\tilde{u}_i - v_i^k\right|\left(\tilde{u}_i - v_i^k\right)dt \tag{4}$$

where N_j is the total number of particles within the solution domain, $\dot{m}_p$ is the mass flow rate along the trajectory of a specific particle, ρ_s is the particle density, C_D is the drag coefficient of spherical particles, and t_{in} and t_{out} are the particle entrance and departure to and from the solution domain.

To investigate the gas flow effects on particle trajectories and the precipitator efficiency, several particles are required to be injected into the domain. This number is determined considering the capacity of the computing equipment. Also, the variety in particle sizes should be considered to predict the submicron- and micron-sized particle precipitation efficiencies. In this study, 100 particle injection points with equal spacing along the inlet boundary were defined and 100 particles, each of a different size, were injected at every injection point. This configuration allows for 10,000 trajectories to be generated and investigated.

Calculation of charges accumulated on the particles is an important aspect to be adopted into ESP numerical modeling. Although there are alternative methods available for this task [25, 26], the charging model developed by Lawless [27] is considered in the present study. As a combined charging model, the Lawless approach involves both field and diffusion effects in calculating the total electrical charge accumulated on each particle. These charging rates are defined as:

$$\frac{dv_f}{d\tau} = \begin{cases} f(w)\dfrac{v-3w}{\exp(v-3w)-1}, & v > 3w \\ \dfrac{3w}{4}(1-\dfrac{v}{3w})^2 + f(w), & -3w \le v \le 3w \\ -v + f(w)\dfrac{-v-3w}{\exp(-v-3w)-1}, & v < -3w \end{cases} \tag{5}$$

$$f(w) = \begin{cases} \dfrac{1}{(w+0.475)^{0.575}}, & w \ge 0.525 \\ 1, & w < 0.525 \end{cases} \tag{6}$$

$f(w)$ is the fractional area function, $v = qe/2\pi\varepsilon_0 d_p kT$ and $w = (K/K+2)(Ed_p e/2kT)$ are the dimensionless particle charge and the electric field strength respectively, and $\tau = (\rho_i b_i t/\varepsilon_0)$ is the dimensionless charging time.

Electric Field and Current Flow

The ionization reactions in the corona discharge are very intricate part of the mathematical model. However, these reactions take place in the very vicinity of the discharge electrode. Considering that fact, many studies involving corona discharges [28, 29, 30] simply ignore the active corona zone; this leads to well-established simplification, which is also utilized in the current work. The electric field is handled via Poisson's equation, which involves ionic-charge density and electric potential:

$$\frac{\partial^2 \varphi}{x_k^2} = -\frac{\rho_{ion} + \rho_{pc}}{\varepsilon_0} \tag{7}$$

where φ is the electric potential (V), ρ_{ion} is the space charge density (C/m^3), ρ_{pc} is the charge density of particles (C/m^3), ε_0 is the permittivity of gas $(C/V \cdot m)$. Also, the convection-diffusion equation is used to calculate space charge density, ρ_{ion}:

$$E_k = -\frac{\partial \varphi}{\partial x_k} \tag{8}$$

$$\frac{\partial}{\partial x_k}\left[\rho_{ion}(k_{ion}E_k + u_k) - D_i\frac{\partial \rho_{ion}}{\partial x_k}\right] = 0 \tag{9}$$

where D_i is the ion diffusion coefficient (m^2/s), k_{ion} is the ion mobility $(m^2/s \cdot V)$ and E_k is the local electric field strength (V/m).

The boundary conditions to solve convection-diffusion equations are required for the electric potential and space charge density. The electric potential is defined on the discharge electrode surfaces, in this case a positive DC voltage, which has a constant value. The collector electrodes, on the other hand, are grounded. The ion density on the discharge electrode surface is calculated using the current value. For the collector electrodes and the remaining boundaries, a steady-state diffusion condition is defined:

$$\rho_w = \frac{J}{\mu_i E_w} \tag{10}$$

where J is the ionic current density on the discharge electrode surface (A/m), and E_w is electric field strength on the discharge electrode surface (V/m). As stated previously, the modeling approach adopted in this study neither involves direct generation and sustaining plasma, nor the relevant chemical reactions. Instead, the electric strength at the corona onset is calculated from Peek's law:

$$E_0 = E_c \delta \left(1 + \frac{c}{\sqrt{\delta r_c}}\right) \tag{11}$$

where E_c is the electric field strength at corona onset, the value of which was assumed to be $3x10^6\ V/m$ in the present study, δ is the relative density compared with the standard condition, c is an empirical constant with a value of 0.0308 and r_c is the discharge electrode radius. Peek's law suggests an iterative approach to solve for the surface electric strength and ion charge density [31]. The iteration is repeated until the electric strength on the wire surface is within a certain tolerance to the value provided by Peek's law. This value is then adopted as the ion charge density on the active electrode on the corona onset. Available numerical studies proved that Peek's law is a successful method of approximating the actual corona discharge conditions [13, 28-30].

Problem Description and Model Discretization

All the above aspects of the numerical modeling, namely electric field calculation, particle charging mechanism, the Lagrangian particle tracking, and the turbulent flow domain for the continuous fluid are calculated with the Comsol Multiphysics software. The multiphysics requirements of ESPs can be handled relatively easily with the software's ability to connect variables of one specific domain to the other, therefore discretizing the problem into multiple branches and multiple study steps, stationary or transient.

The study requires a turbulence scheme to comply with the local Re numbers that may well exceed the laminar flow limitations in the ESP domain. Turbulent flow through ESP is calculated via the Standard $k-\varepsilon$ model. The electric field and the ionic charge density, resulting from a steady-state Poisson solver, were imported to the fluid flow interface to handle the particle charging and particle transport. A transient solver with 1ms time steps is considered to obtain particle behavior, particle charging characteristics, and eventually the ESP efficiency. In the current study, the ESP domain is initialized with a set of boundary conditions, providing information on the turbulent flow and electrostatics aspects of the model. The airflow within the domain is solved first, without accounting for the effects of the corona discharge. The electric field strength is calculated via the Poisson equation, which requires the space charge density to be determined (Eqs.s 7 and 8). The initial ion charge density at the active electrode surface is assumed to be zero. From this point, the surface ion density is updated iteratively. When the surface field strength is within a certain tolerance with the iterative result, the final value of the surface charge density is adopted for the remaining of the numerical calculation [32].

Following the turbulent flow and electric field calculations, particles from the precipitator inlet are injected into the domain, where each particle trajectory is calculated based on the Lagrangian scheme, and particle fates are calculated by the software. Because the behavior of charged particles may affect the flow patterns inside the ESP domain, the calculations were repeated multiple times, by using the convergent results of the latest simulation run. This way, the electrical body forces and particle charge densities are updated until the set of equations is conveniently converged. The model is based on a simplified, 2D ESP geometry, containing two planar ground electrodes and 4 active electrodes with 2mm diameter (Fig. 1). A positive DC electrical potential of 43.5 kV is applied to the active electrodes. Due to the mass properties of the particles, the electric field effects on the particles are dominant, compared to gravitational effects, hence the effect of gravity on the particles is neglected. The forced convection of air is defined as a fully developed flow with 1m/s average velocity at the inlet boundary of the model. The geometry

has an active precipitation area of $0.14m^2$ (Fig. 1 (a)), with a channel width (W) of 610mm and a height ($2H$) of 230mm. Expecting an electric field with strong gradient, a triangular mesh with a relatively low growth rate is employed. After discretization, the domain comprises 281,610 elements with an average element quality of 0.89. The overall view of the applied mesh can be seen on Fig. 1 (b). The mesh structure exhibits a densely-packed discretization in the vicinity of the corona electrodes, capturing both electrostatic properties and the particle trajectories reliably, as will be seen in the following pages.

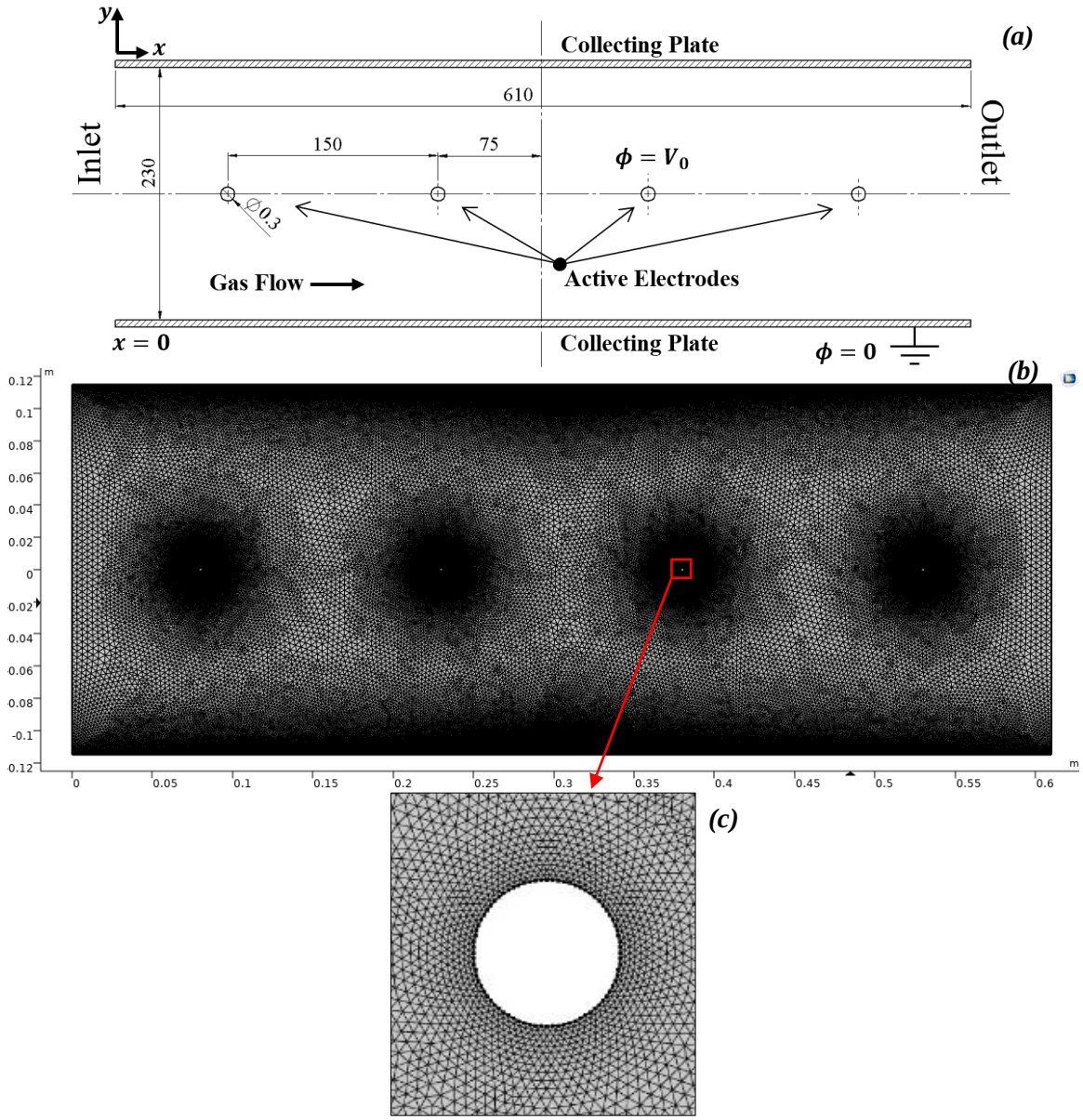

Figure 1. (a) The Model Geometry and **(b)** Mesh Structure with a Close-up View of Edge Division **(c)** Near Corona Electrodes.

The boundaries and their values are summarized on Table 1. One important aspect is that, the electric field strength at all active electrode surfaces are the values that satisfy Peek's law approach employed in this study. The electric potential to commence the ESP process is directly adopted from the commonly-cited work of Penney and Matick [33].

Table 1. Boundaries Conditions for the Simulated ESP Configuration

	Electric Field	*Space Charge Density*	*Fluid Flow*	*Particle Tracking*
Inlet	$\partial\varphi/\partial n = 0$	$\partial\rho_{ion}/\partial n = 0$	$v_x = 1\ m/s$ $v_y = 0.0\ m/s$	$u_x = 1\ m/s$ $u_y = 0.0\ m/s$
Outlet	$\partial\varphi/\partial n = 0$	$\partial\rho_{ion}/\partial n = 0$	0 Pa (Gage Pressure)	Vanish (Particle Counter)
Ground Electrodes	$\varphi = 0\ kV$	$\partial\rho_{ion}/\partial n = 0$	No slip.	Freeze
Active Electrodes	$\varphi = 43.5kV$	Determined Iteratively	No slip.	Freeze

Finally, the particles injected from the inlet boundary of ESP domain are of the uniform 1500 kg/m3 density [34]. To properly address the submicron and micron range particle behaviors within the model, a uniform distribution of particles sizes, between 50nm and 10μm containing 100 different diameters is adopted.

RESULTS AND DISCUSSION

The numerical results for the electric potential distribution in the investigated model were compared with the seminal work published by Penney and Matick [33]. The electric potential distribution observed in the present study is in good agreement with the said publication (Fig. 2).

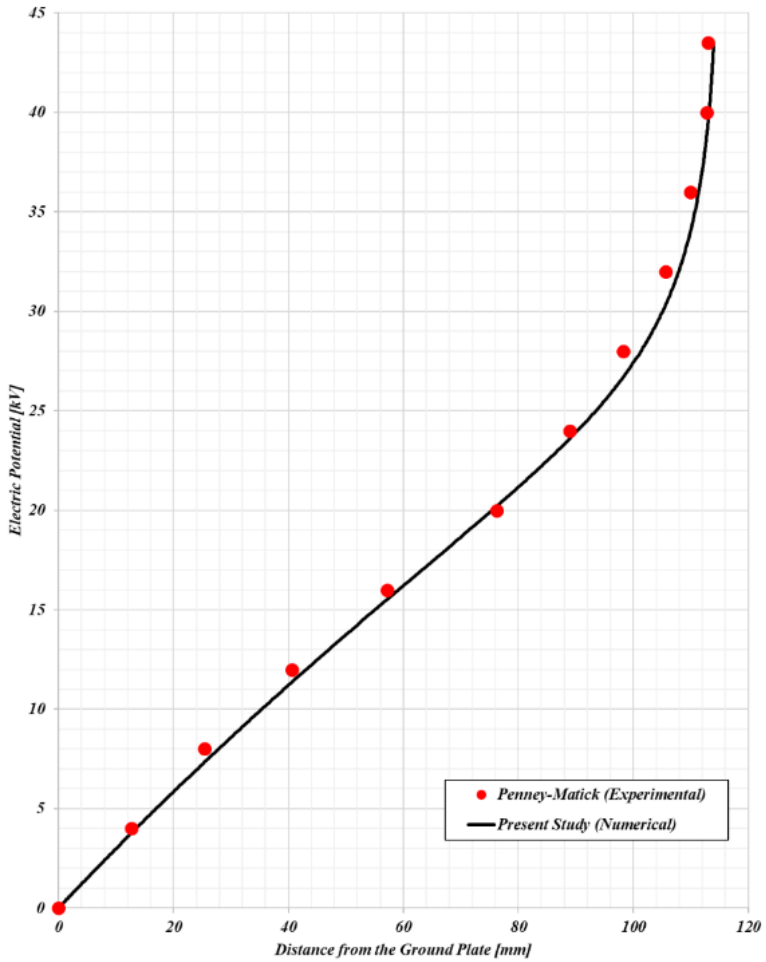

Figure 2. Electric Potential Distribution Calculated Numerically Against the Experimental Results Published by Penney and Matick [33].

Adequate mesh refinement and mesh independence in the numerical study was also an important aspect of model validation. Too coarse a mesh possibly provides a faster solution -even convergence, but the parametric results may not display the best results in terms of model stabilization. Too fine mesh metrics, the model might display redundancy in terms of degrees of freedom, and poor convergence time. To provide a better tradeoff between refinement and model stability, multiple mesh structures with varying metrics were applied. The critical parameter was assumed to be space charge density (C/m^3) in the corona electrode vicinity and the results suggested that the adopted mesh suggests an optimum refinement (Table 2). Fig 3 shows no significant improvement in the parameter with advancing refinement in comparison to the adopted mesh configuration. To note, mesh metrics are scored between 0-1, with 1 (or 100%) being the best possible configuration for a given metric. Skewness penalizes elements with extremely low or high angles compared to an ideal element, whereas volume versus circumradius evaluates the proportion of an element area and the circumscribed circle of the element.

Table 2. Results of Different Mesh Configurations Utilized in Mesh Independence Study.

Mesh Configuration	Space Charge Density [C/m^3]	Maximum Element Size [mm]	Growth Rate	# of Elements	Average Skewness	Volume versus circumradius
Finer 3	3.2190E-05	4	1.03	510948	0.9105	0.9634
Finer 2	3.2184E-05	5	1.04	362484	0.9027	0.9545
Finer 1	3.2185E-05	6	1.045	316534	0.8971	0.9491
Adopted Mesh	**3.2187E-05**	**7.5**	**1.05**	**281610**	**0.8946**	**0.9456**
Coarser 1	3.2219E-05	10	1.1	138774	0.8674	0.9095
Coarser 2	3.2337E-05	15	1.2	76122	0.8365	0.86
Coarser 3	3.2666E-05	20	1.3	56704	0.8249	0.831

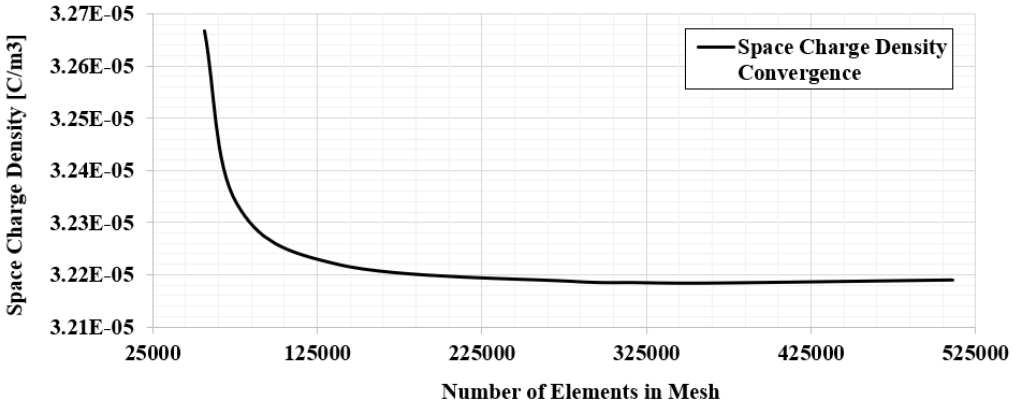

Figure 3: The Optimum Mesh Configuration Was Determined Considering the Largest Maximum Element Size (7.5mm in This Study) That Conforms the Results Calculated via Further-refined Alternatives.

The electric field intensity significantly varies at different points of the precipitation channel (Fig. 4). This variation is much stronger close to the channel symmetry plane and is much milder near the collecting electrodes. As it can be seen on Fig. 5, the electric field variation results in a variable ion charge distribution, which affects the particle charging level.

The ionic density shows a similar behavior to the electric field intensity; it reaches the peak the highest values in the vicinity of discharge electrodes. As it can be seen on Fig. 4, near the first electrode the charge density is about $2.58x10^{-5}$ C/m^3. The same can also be observed for other lines along the precipitation channel. Another important aspect of the plot is that the maximum charge densities are observed at both ends of the precipitation channel with smaller values at the center. Ionic charge densities tend to concentrate near the discharge electrodes, but these densities preserve their values along the vertical distance from corona electrodes; namely $5.35x10^{-6}$ C/m^3 for H/4, $5.34x10^{-6}$ C/m^3 for H/2 and $5.06x10^{-6}$ C/m^3 for 3H/4. This mechanism guarantees the diffusion charging of submicron particles along the precipitation channel of the ESP.

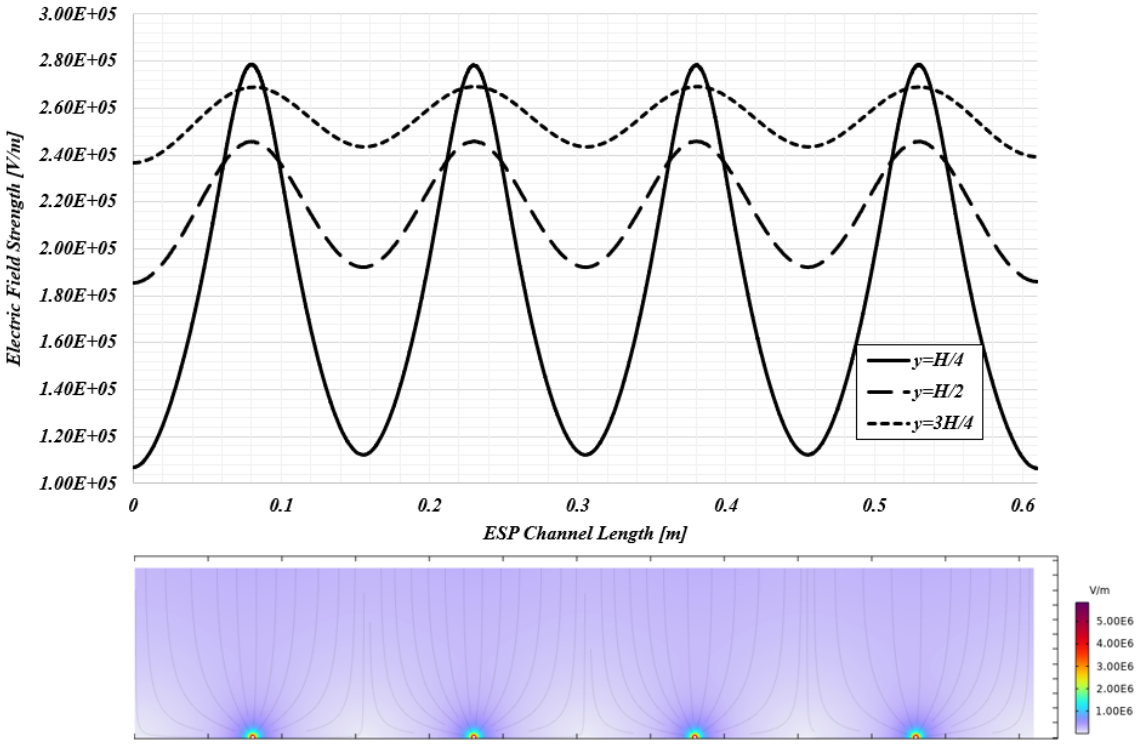

Figure 4. Magnitude of Electric Field at 43.5kV Corona Electrode Voltage. The Plot Shows Field Values on Three Lines Along the ESP Channel **(Top)**, Compared to the Contour Graph on Electric Field Magnitude **(Bottom)**.

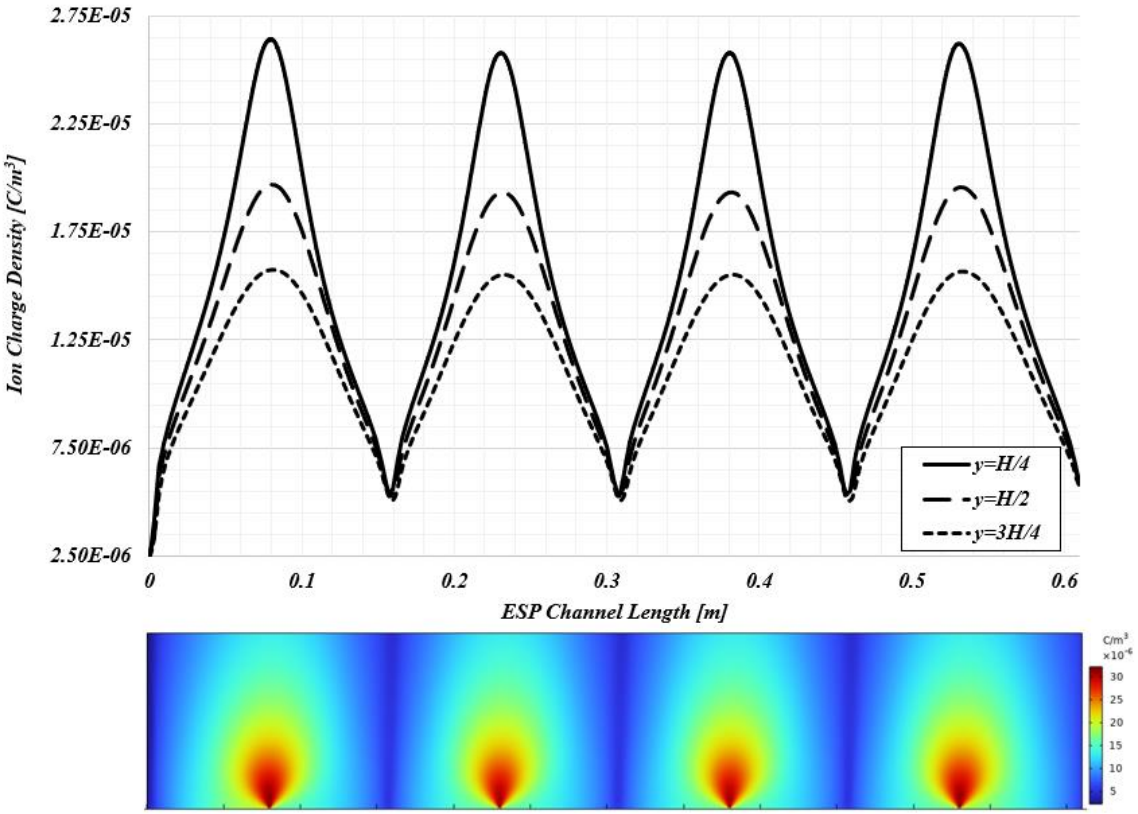

Figure 5. Ionic Charge Density Along Three Different Horizontal Lines (top) and in the Entire Precipitation Channel (bottom).

Despite of the fact that a large variety in particle sizes (50nm-10µm) were utilized in this study to investigate precipitation efficiency, three specific particle diameters are picked to demonstrate the field and diffusion charging mechanism effects. When a diameter smaller than 1µm is considered, the diffusion effect dominates the charge accumulated on the particles. As seen on Fig. 6(a), diffusion charging practically determines the charge number as particles with a diameter of 50nm travel through ESP domain. However, this scheme changes with the increasing particle size. As particle sizes go from submicron to micron level, field charging mechanism becomes more and more prominent, as seen on Figs. 6(b) and (c). For relatively large particles, the charge accumulated on the particle is largely attributed to the field charging, yet the diffusion part is also still significant [35, 36].

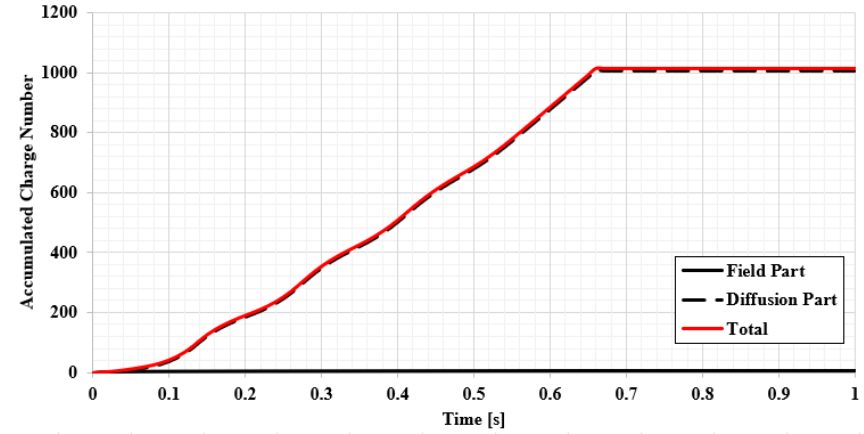

(a)

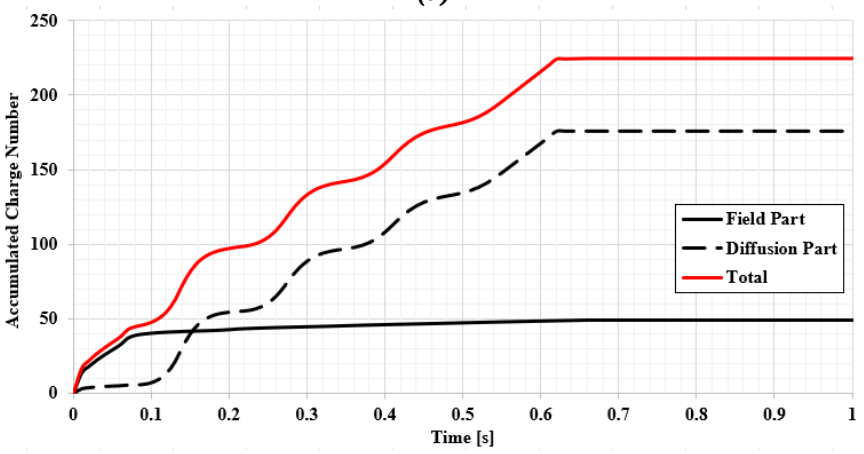

(b)

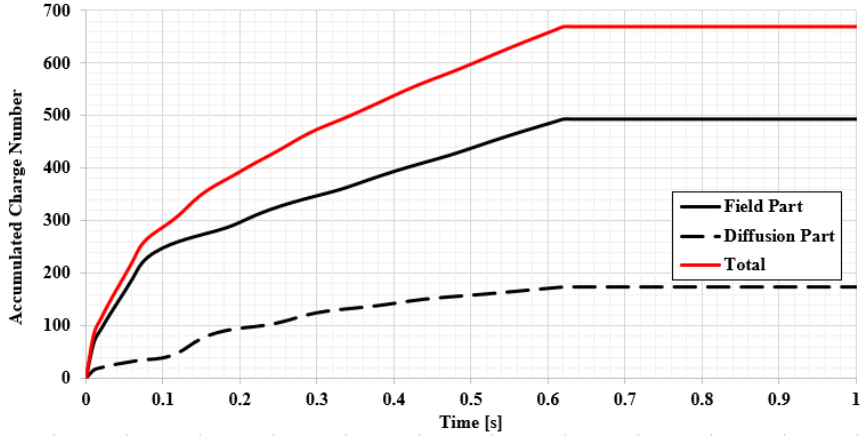

(c)

Figure 6. The Dynamics of the Accumulated Charge for the Two Charging Mechanisms **(a)** 50nm, **(b)** 1µm, **(c)** 5µm Diameter.

The current study assumes a 43.5kV voltage applied to four discharge electrodes and a constant discharge current of 0.475mA. Also, the electrical charging of particles was defined by a dimensionless charge number. The precipitation efficiency of submicron particles sharply decreases for particle diameters between 50nm and 250nm. With an increasing particle size the precipitation efficiency increases to around 18% for 1μm diameter particles. This variation is also encountered in previous studies [30, 37] both experimental and numerical, and can be accounted to the charging mechanism that is effective for a given size range of particles. The diffusion charging becomes the dominant mechanism with small particle size, as stated previously. Higher numbers of accumulated charge, combined with the relatively high electric field intensity near the inlet boundary of ESP results in better precipitation efficiencies for 50nm particles (Fig. 6(a)). This property of the process changes and the efficiency drops with increasing particle size for submicron range. However, as field charging mechanism becomes dominant for particles larger than 1μm, the efficiencies increase and over 77% of particles with diameters 5μm or larger are precipitated (Fig. 7(b)).

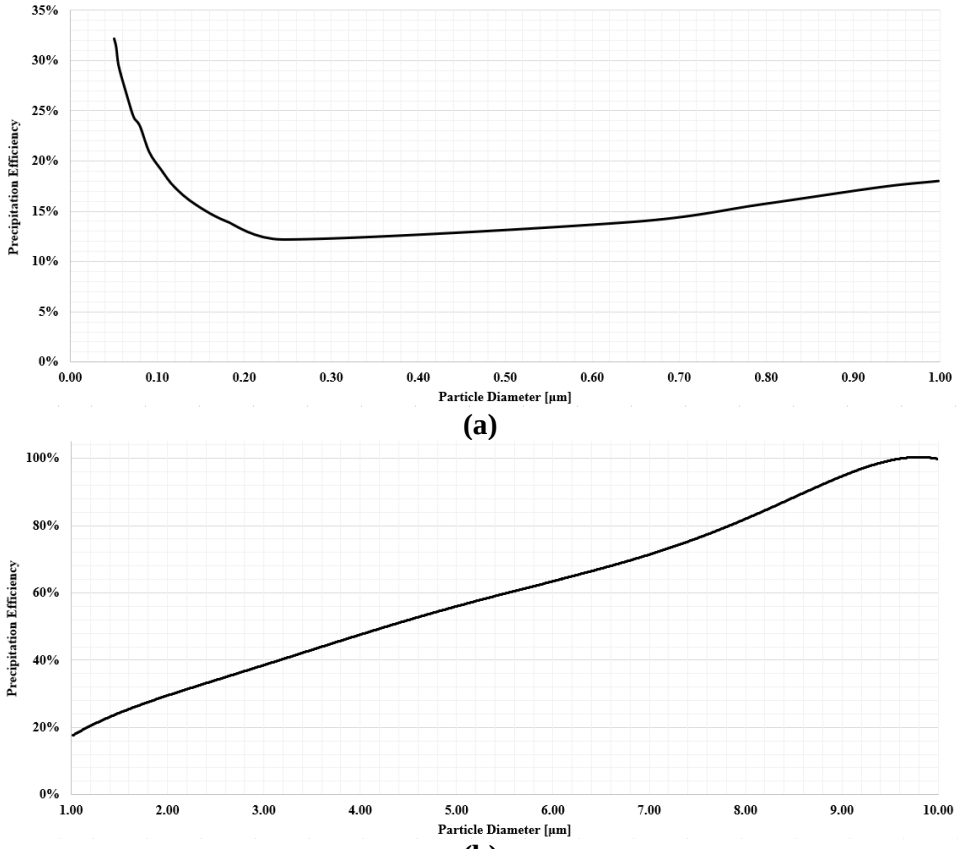

Figure 7. The Relation Between the Precipitation Efficiency and Particle Size: Submicron-sized Particles (a) and Micron-sized Particles (b).

CONCLUSION

In this study, the charging of micron- and submicron-sized particles and particle trajectories were investigated in a wire-to-plate DC electrostatic precipitator by developing a numerical model validated against published experimental data. The effect of different charging mechanisms is discussed using a simplified corona discharge process, along with the characteristics of electric field distribution. Based on the analysis, the following conclusions can be stated. The electric field and ion charge density along the length of precipitation channel displays large variations. However, following the first discharge electrode, the ion charge density remains above a certain level for the entire of channel length. This is a main factor for maintaining particle charge accumulation required for higher precipitation efficiencies, especially for micron-sized particle range.

While submicron particles are mostly affected by the diffusion effects, this mechanism changes with an increasing particle size. For particles with 1μm and larger diameters, the field charging mechanism becomes dominant, but with diffusion charging effects still significant. On the other hand, the field charging is largely ineffective when submicron sizes are in question. Finally, an increasing particle diameter results in both charging mechanisms become more effective, thus improving the overall precipitation efficiency within the ESP channel. However, for the submicron

range, efficiencies averaging 21% were observed, because the field charging is nearly absent in charging these particles. The study is distinguishable by the detailed, numerical field investigation of electrical parameters with a model validated against the actual experimental data. A novel perspective to separating the effects of the field and diffusion charging mechanisms on particle precipitation is also suggested in the context.

ACKNOWLEDGMENTS

The author would like to thank TUBITAK-BIDEB for making this work possible, under the roof of 2219-International Postdoctoral Research Fellowship Program (Grant No: 1059B192100001).

CONFLICT OF INTERESTS

The author declares that he has no known competing financial interests or personal relationships that could have appeared to influence the work reported in this paper.

REFERENCES

[1] White H.J. Industrial electrostatic precipitation, 1st ed. (1963), Reading, MA, USA: Addison-Wesley Pub. Co. ISBN-13: 978-0201086508

[2] Mizuno, A. Electrostatic precipitation. *IEEE Transactions on Dielectrics and Electrical Insulation*, vol. 7, no. 5 (2000), pp. 615-624. https://doi.org/10.1109/94.879357

[3] Marquard A., Kasper M., Meyer J., Kasper G. Nanoparticle charging efficiencies and related charging conditions in a wire-tube ESP at DC energization. *Journal of Electrostatics*, vol. 63, no. 1 (2005), pp. 693–698. http://dx.doi.org/10.1016/j.elstat.2005.03.032

[4] Y. Kawada, Y., Kaneko, T., Ito T., Chang, JS. Simultaneous removal of aerosol particles, NOx and SO2 from incense smokes by a DC wire-plate electrostatic precipitator under positive coronas. *Journal of Aerosol Science*, vol. 32, no. 1 (2001), pp. 945-946. http://dx.doi.org/10.1016/S0021-8502(21)00425-0

[5] Y. P. Raizer, Gas Discharge Physics, 1st ed., Heidelberg, Germany: Springer (1991), pp. 324-375. ISBN-13: 978-3642647604

[6] Bologa, A., Paur, HR., Seifert, H., Woletz, K. Influence of gas composition, temperature and pressure on corona discharge characteristics. *International Journal of Plasma Environmental Science and Technology*, vol. 5, no.1 (2011), pp. 110–116.

[7] Xu X., Gao X., Yan P., Zhu W., Zheng, C., Wang, Y. Particle migration and collection in a high-temperature electrostatic precipitator. *Separation and Purification Technology*, vol. 143, no. 1 (2015), pp. 184–191. http://dx.doi.org/10.1016/j.seppur.2015.01.016

[8] Xiao, G., Wang, X., Zhang, J., Ni, M., Gao, X., Cen, K. Characteristics of DC discharge in a wire-cylinder configuration at high ambient temperatures. *Journal of Electrostatics*, vol. 72, no. 1 (2014), pp. 13–21. http://dx.doi.org/10.1016/j.elstat.2013.10.013

[9] Xiao, G., Wang, X, Yang, G., Ni, M., Gao, X., Cen, K. An experimental investigation of electrostatic precipitation in a wire–cylinder configuration at high temperatures. *Powder Technology*, vol. 269, no. 1 (2015), pp. 166–177. https://doi.org/10.1016/j.powtec.2014.08.063

[10] Soldati, A. On The Effects of Electrohydrodynamic Flows and Turbulence on Aerosol Transport and Collection in Wire-Plate Electrostatic Precipitators, *Journal of Aerosol Science*. Vol. 31, No. 3 (2000), pp. 293-305. http://dx.doi.org/10.1016/S0021-8502(99)00055-5

[11] Kumar, A., Parihar, S., Hammer, T., Sridhar, G. Development and testing of tube type wet ESP for the removal of particulate matter and tar from producer gas. *Renewable Energy*, vol: 74, no. 1 (2015), pp. 875-883. http://dx.doi.org/10.1016/j.renene.2014.09.006

[12] Nikas, KSP., Varonos, AA., Bergeles, GC. Numerical simulation of the flow and the collection mechanisms inside a laboratory scale electrostatic precipitator. *Journal of Electrostatics*, vol 63, no. 5 (2005), pp. 423-443. http://dx.doi.org/10.1016/j.elstat.2004.12.005

[13] Gao, W., Wang, Y., Zhang, H., Guo, B., Zheng, C., Guo, J., Gao, X., Yu, A. Numerical simulation of particle migration in electrostatic precipitator with different electrode configurations. *Powder Technology*, vol. 361, no. 1 (2020), pp. 238-247. http://dx.doi.org/10.1016/j.powtec.2019.08.046

[14] Zhao, L., Adamiak, K. EHD Flow in Air Produced by Electric Corona Discharge in Pin-Plate Configuration. *Journal of Electrostatics*, 63 (2005), pp. 337–350. https://doi.org/10.1016/j.elstat.2004.06.003

[15] Böttner, C.U. The role of the space charge density in particulate processes in the example of the electrostatic precipitator. *Powder Technology*, vol. 136, no. 1 (2003), pp. 285-294. http://dx.doi.org/10.1016/j.powtec.2003.08.020
[16] Wang, X. Effects of corona wire distribution on characteristics of electrostatic precipitator. *Powder Technology*, vol. 366, no. 1 (2020), pp. 36-42. http://dx.doi.org/10.1016/j.powtec.2020.02.044
[17] Blazek, J. Chapter 7 – Turbulence Modeling. in Computational Fluid Dynamics: Principles and Applications, 3rd ed., Oxford, UK: Butterworth-Heinemann (2015), pp. 213-252. http://dx.doi.org/10.1016/B978-0-08-044506-9.X5000-0
[18] Gui, N., Jiang, S., Tu, J., Yang, X. Chapter 4 - Application in gas-particle flows. Gas-Particle and Granular Flow Systems, 1st ed., Amsterdam, The Netherlands: Elsevier (2020), pp. 123-205. http://dx.doi.org/10.1016/B978-0-12-816398-6.00013-4
[19] Durst, F., Milojevic, D., Schonung, B. Eulerian and Lagrangian predictions of particulate two-phase Flows: A numerical study. *Applied Mathematical Modelling*, vol. 8, no. 1 (1984), pp. 101-115. https://doi.org/10.1016/0307-904X(84)90062-3
[20] Xu, Z., Han, Z., Qu, H. Comparison between Lagrangian and Eulerian approaches for prediction of particle deposition in turbulent flows. *Powder Technology*, vol. 360, no. 1 (2020), pp. 141-150. https://doi.org/10.1016/j.powtec.2019.09.084
[21] Sun, Z., Zhu, J., Zhang, C., Numerical study on the hydrodynamics in high-density gas-solid circulating fluidized bed downer reactors. *Powder Technology*, vol. 370, no. 1 (2020), pp. 184-196. http://dx.doi.org/10.1016/j.powtec.2020.05.035
[22] Ma, C., Zhou, Y., Wang, J., Li, X. Numerical study on solar spouted bed reactor for conversion of biomass into hydrogen-rich gas by steam gasification. *International Journal of Hydrogen Energy*, vol. 45, no. 58 (2020), pp. 33136-33150. http://dx.doi.org/10.1016/j.ijhydene.2020.09.120
[23] Yang, S., Dong, R., Du, Y., Wang, S., Wang, H., Numerical study of the biomass pyrolysis process in a spouted bed reactor through computational fluid dynamics. *Energy*, vol. 214, no. 1 (2021), pp. 1-15. http://dx.doi.org/10.1016/j.energy.2020.118839
[24] Adeniji-Fashola, A., Chen, CP. Modeling of confined turbulent fluid-particle flows using Eulerian and Lagrangian schemes. *International Journal of Heat and Mass Transfer*, vol: 33, no. 1 (1990), pp. 691-701. https://doi.org/10.1016/0017-9310(90)90168-T
[25] Li, L., Gopalakrishnan, R. An experimentally validated model of diffusion charging of arbitrary shaped aerosol particles. *Journal of Aerosol Science*, vol: 151, no. 1 (2021), pp. 1-28. http://dx.doi.org/10.1016/j.jaerosci.2020.105678
[26] Zhu, Y., Chen, C., Chen, M., Shi, J., Shangguan, W. Numerical simulation of electrostatic field and its influence on submicron particle charging in small-sized charger for consideration of voltage polarity. *Powder Technology*, vol: 380, no. 1 (2021), pp. 183-198. https://doi.org/10.1016/j.powtec.2020.11.042
[27] Lawless, PA. Particle charging bounds, symmetry relations, and an analytic charging rate model for the continuum regime. *Journal of Aerosol Science*, vol. 27, no. 2 (1996), pp. 191-215. https://doi.org/10.1016/0021-8502(95)00541-2
[28] Ramadhan, AA., Kapur, N., Summers, JL., Thompson, HM. Numerical development of EHD cooling systems for laptop applications. *Applied Thermal Engineering*, vol. 139, no. 1 (2018), pp. 144-156. http://dx.doi.org/10.1016/j.applthermaleng.2018.04.119
[29] Long, HGZ., Feng, Z., Lin, B., Yu, T. Numerical simulation of the characteristics of oil mist particles deposition in electrostatic precipitator. *Process Safety and Environmental Protection*, vol. 164, no. 1 (2022), pp. 335-344. http://dx.doi.org/10.1016/j.psep.2022.06.022

[30] Lu, Q., Yang, Z., Zheng, C., Li, X., Zhao, C., Xu, X., Gao, X., Luo, Z., Ni, M., Cen, K. Numerical simulation on the fine particle charging and transport behaviors in a wire-plate electrostatic precipitator. *Advanced Powder Technology*, vol. 27, no. 5 (2016), pp. 1905-1911. http://dx.doi.org/10.1016/j.apt.2016.06.021

[31] Peek, F.W., Dielectric Phenomena in High-voltage Engineering (1929), McGraw-Hill Book Company, Inc. ISBN-13: 978-1443732321

[32] Cross, J. Electrostatics: Principles, Problems and Applications, 1st ed. (1987), Bristol, UK: CRC Press. ISBN-13: 978-0852745892

[33] Penney GW., Matick, RE. Potentials in D-C corona fields. *Transactions of the American Institute of Electrical Engineers, Part I: Communication and Electronics*, vol. 79, no. 2 (1960), pp. 91-99. https://doi.org/10.1109/TCE.1960.6368550

[34] Choi, BS., Fletcher, CAJ. Turbulent particle dispersion in an electrostatic precipitator. *Applied Mathematical Modelling*, vol. 22, no. 12 (1998), pp. 1009-1021. https://doi.org/10.1016/S0307-904X(98)10034-3

[35] Lackowski, M., Krupa, A., Jaworek, A. Corona discharge ion sources for fine particle charging. *Journal of Electrostatics*, vol. 72, no. 2 (2010), pp. 377-382. http://dx.doi.org/10.1140/epjd/e2009-00309-0

[36] Zhang, K., Chen, S., Long, T., Xu, M., Zhang, H., Zhang, D. Study on Mechanism and Characteristics of Particle Charging in Electrostatic Precipitator. *IOP Conference Series: Materials Science and Engineering*, vol. 677, no. 1 (2019), pp. 1-8. http://dx.doi.org/10.1088/1757-899X/677/3/032109

[37] Byeon, JH., Hwang, J., Park, JH., Yoon, KY., Ko, BJ., Kang, SH., Ji, JH. Collection of submicron particles by an electrostatic precipitator using a dielectric barrier discharge. *Journal of Aerosol Science*, vol: 37, no. 11 (2006), pp. 1618-1628. http://dx.doi.org/10.1016/j.jaerosci.2006.05.003